Random barrier height model for phase shifted conductivity in perovskites

Authors: V. Hugo Schmidt, G.F. Tuthill, C.-S. Tu, T.V. Schogoleva, and S.C. Meschia

This is an Accepted Manuscript of an article published in Ferroelectrics in 1997, available online: http://www.tandfonline.com/10.1080/00150199708213428.

V.H. Schmidt, G.F. Tuthill, C.-S. Tu, T.V. Schogoleva, and S.C. Meschia, “Random barrier height model for phase shifted conductivity in perovskites,” Ferroelectrics 199, 51-67 (1997).

RANDOM BARRIER HEIGHT MODEL FOR PHASE SHIFTED CONDUCTIVITY IN PEROVSKITES

V. H. SCHMIDT, G. F. TUTHILL, C.-S. TU*,
T. V. SCHOGOLEVA† and S. C. MESCHIA

Physics Dept., Montana State Univ., Bozeman, MT 59717, USA

(Received in final form 15 August 1996)

A large dielectric permittivity peak which occurs at low frequency and high temperature in many perovskite crystals and ceramics, and an associated difference in dc and ac conductivity, is attributed to phase shifted conductivity resulting from mobility barriers of different heights. A model is developed which has intrinsic barriers, and higher and more widely spaced extrinsic barriers, and special cases are examined. Model predictions show good agreement with experimental results of Stumpe, Wagner, and Bäuerle for an $SrTiO_3$ single crystal 1.02 mm thick. The additional peaks seen by them at higher temperature for a crystal 0.24 mm thick are qualitatively accounted for by adding a third set of still higher barriers with spacing equal to the crystal thickness.

Keywords: Perovskites; conductivity; dielectric permittivity

INTRODUCTION

In recent years it has become apparent that a wide range of perovskite crystals and ceramics exhibit a large dielectric peak at low frequencies and high temperatures. These materials include crystals of strontium titanate[1], barium titanate[1,2], lead titanate[2,3], the relaxor ferroelectric NBT ($Na_{1/2}Bi_{1/2}TiO_3$)[4,5], and various ceramics[2,3]. In some cases, this peak was attributed to relaxor ferroelectric behaviour[3,4]. However, it is seen

*Now at Fu Jen University, Taipei, Taiwan.
†Now at 3rd Frunzenskaya St., 7, Apt. 87, Moscow, Russia.

also in crystals which have no ferroelectric transition. Even at the peaks of these large permittivities, the loss tangent is generally larger than unity. This raised the suspicion that these dielectric peaks are associated with the conduction mechanism,[2,5,6] by means of a phase-shifted conductivity.

In previous papers, we discussed some of these results and various explanations of these phenomena.[4-6] We made a partial presentation of our present model previously,[6] but here we describe the model and work through the equations in detail, and present several limiting cases. Finally, we make comparison with experimental results of Stumpe, Wagner, and Bäuerle[1] for $SrTiO_3$, which provides a clear-cut test because there are no ferroelectric or other transitions to complicate the dielectric behavior in the temperature range of interest, which lies above room temperature.

MODEL

To explain these phenomena using a one-dimensional model, we make the following assumptions:

The conductivity is extrinsic, with n carriers of charge q per unit volume, n being independent of temperature T.

There are intrinsic barriers of height B (in temperature units) giving a thermally activated intrinsic mobility. These barriers are spaced a distance a apart, where a is of the order of a lattice cosntant, as shown in Figure 1.

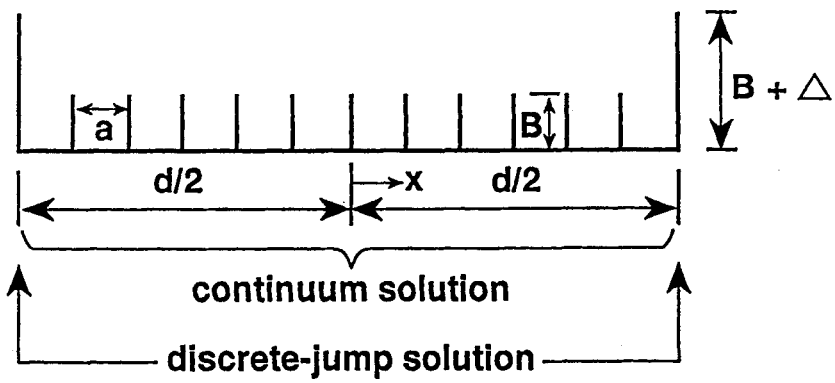

FIGURE 1 Illustration of barrier heights and spacing for our model.

There are extrinsic barriers every distance d, of height $B + \Delta$. The attempt frequency for crossing the barriers is $\nu = k\Theta/h$, where Θ is the Debye temperature.

The material is of infinite extent.

To find the complex ac conductivity $\sigma(\omega) = \sigma'(\omega) + i\sigma''(\omega)$ for this model, we use the defining relation

$$\sigma(\omega) = (J + \partial D/\partial t)/\langle E \rangle. \tag{1}$$

J is the conduction current density and $\partial D/\partial t$ the displacement current density which are present when an electric field with time dependence $e^{i\omega t}$ is applied to the sample. Both of these currents separately depend on position as well as time, but their sum, the total current $J_t = J + \partial D/\partial t$, is independent of position, as required by electrodynamics. J_t is equal to the measured instantaneous current divided by the electrode area. The electric field E is also position-dependent, but the measured instantaneous voltage is the spatial average $\langle E \rangle$ of the field, multiplied by the crystal thickness between the electrodes. In general, the instantaneous current and voltage are out of phase, yielding a complex ac conductivity $\sigma(\omega)$.

To find the complex permittivity $\varepsilon(\omega)$ we then use the fact that $\sigma(\omega)$ and $\varepsilon(\omega)$ are related by

$$\varepsilon(\omega) = \varepsilon'(\omega) - i\varepsilon''(\omega); \quad \varepsilon' = \sigma''/\varepsilon_0\omega, \quad \varepsilon'' = \sigma'/\varepsilon_0\omega, \tag{2}$$

where ε_0 is the MKS constant 8.85×10^{-12} C^2/Nm^2.

We proceed by first noting that it is sufficient to consider a single interval of width d in the material. Placing higher barriers at $x = \pm d/2$, we make the approximation that the material in the interval $-d/2 < x < d/2$ can be treated as a continuum. We find equations relating $E(x,t)$, $J(x,t)$, $\rho(x,t)$, and the high frequency conductivity σ_∞, and from these obtain a differential equation for $\rho(x,t)$. We find the general solution for ρ, and put in the boundary condition relating E, J, and ρ at the high barriers to determine the particular solution. The electric displacement $D(x,t)$ is found from E by $D = \varepsilon_0\varepsilon'(\infty)\, E \equiv \varepsilon_\infty E$, where $\varepsilon'(\infty)$ is the "background" relative permittivity, and is the only significant contribution to permittivity at high ("∞") frequencies.

Note that ρ must be an odd function of x, so that its spatial average is zero (as required for a crystal with overall electrical neutrality), while E is an even function of x. The conduction current density J and displacement current density $\partial D/\partial t$ are both even functions of x.

We begin the derivation of the continuum equations by finding an expression for the conduction current density $J(x,t)$:

$$J = \sigma_\infty E - \bar{D}\,\partial\rho/\partial x \tag{3}$$

$$= \sigma_\infty E - \mu kT(\partial\rho/\partial x)/q$$

$$= \sigma_\infty E - \sigma_\infty \tau\,\partial\rho/\partial x.$$

We obtain the second equality above by substituting the Einstein relation $q\bar{D} = \mu kT$ and the third by substituting $\sigma_\infty = nq\mu$. Here $\bar{D}$ is the diffusion coefficient, k is Boltzmann's constant, and the quantity $\tau = kT/nq^2$ has the dimension of (length)$^{-2}$. The thermally activated mobility μ is given by $\mu = v_d/E$, where v_d is the drift velocity. We may write v_d as the attempt frequency ν multiplied by the jump distance a, and by the difference

$$\exp[(-kB + qEa/2)/kT] - \exp[(-kB - qEa/2)/kT]$$

$$\simeq (qEa/kT)\exp(-B/T) \tag{4}$$

in jump success probability for jumps along and against E. Because the phenomena of interest occur above the Debye temperature Θ, we assume $\nu = k\Theta/h$, where h is Planck's constant.

Putting all these factors together, we find

$$\sigma_\infty = (nq^2a^2\Theta/hT)\exp(-B/T) \tag{5}$$

for the conductivity at frequencies high enough that the extrinsic barriers of height $B + \Delta$ have negligible effect.

Now we find the remaining continuum equations for the region $-d/2 < x < d/2$ between the high barriers. We start by taking the x derivative of Eq. (3) and rearranging:

$$\partial E/\partial x = (\partial J/\partial x)/\sigma_\infty + \tau\partial^2\rho/\partial x^2. \tag{6}$$

We can eliminate E by combining Eq. (6) with the equation

$$\partial E/\partial x = \rho/\varepsilon_\infty, \tag{7}$$

which is Gauss's Law in one dimension. To eliminate J, we substitute into Eq. (6) the one-dimensional continuity equation

$$\partial J/\partial x = -\partial \rho/\partial t. \tag{8}$$

Making these substitutions, we obtain the fundamental differential equation governing the charge density $\rho(x,t)$:

$$\partial^2 \rho/\partial x^2 - \rho/\varepsilon_\infty \tau - (\partial \rho/\partial t)/\sigma_\infty \tau = 0 \tag{9}$$

This equation is separable, and we may assume

$$\rho(x,t) = f(x) e^{+i\omega t}. \tag{10}$$

The + sign choice in the exponential is consistent with the usual choice of a + sign in $\sigma = \sigma' + i\sigma''$ and the corresponding − sign in $\varepsilon = \varepsilon' - i\varepsilon''$. The spatial dependence of ρ is then determined by the equation

$$\partial^2 f/\partial x^2 = \alpha^2, \tag{11}$$

where

$$\alpha = [(1/\varepsilon_\infty \tau)^2 + (\omega/\sigma_\infty \tau)^2]^{1/4} \exp[(i/2)\tan^{-1}(\omega \varepsilon_\infty/\sigma_\infty)] \tag{12}$$

Eq. (11) has the general solution

$$f(x) = A' e^{\alpha x} + A'' e^{-\alpha x}, \tag{13}$$

where constants A' and A'' must be determined by boundary conditions. For overall charge neutrality, the integral of f from $-d/2$ to $d/2$ must vanish, which requires that $A'' = -A'$. Thus, setting $A' = A/2$,

$$\rho(x,t) = A \sinh(\alpha x) e^{i\omega t}. \tag{14}$$

From here on, the time dependence $e^{i\omega t}$ will be omitted in expressions for ρ, J, and E.

We next need to find expressions for the total current J_t and for the average field $\langle E \rangle$. Since J_t is position-independent, we choose to calculate its constituents J and $\partial D/\partial t$ at the high barriers.

The boundary condition at the high barriers has the form of Eq. (3) for $J(\pm d/2)$, but with two substitutions. First, σ_∞ is replaced by $\sigma_\infty e^{-\Delta/T}$ because these barriers are an amount Δ higher. Second, $\partial\rho/\partial x$ for this situation is approximated by the charge density difference $\rho(-d/2) - \rho(d/2)$ for the sites adjacent to the barrier, divided by the separation a of these sites. With these substitutions, this equation becomes

$$J(\pm d/2) = \sigma_\infty e^{-\Delta/T}\{E(\pm d/2) - \tau[\rho(-d/2) - \rho(d/2)]/a\}$$

$$= \sigma_\infty e^{-\Delta/T}\{E(\pm d/2) + 2\tau a^{-1} A \sinh b\}, \tag{15}$$

where $b = \alpha d/2$

Our other relation needed to find $J(\pm d/2)$ and $E(\pm d/2)$ in terms of the arbitrary constant A is the continuum relation for J in Eq. (3), evaluated at $x = \pm d/2$:

$$J(\pm d/2) = \sigma_\infty[E(\pm d/2) - \tau A \alpha \cosh b], \tag{16}$$

where we have used $\partial\rho/\partial x = A\alpha\cosh(\alpha x)$. Eliminating $J(\pm d/2)$ between Eqs. (15) and (16) yields

$$E(\pm d/2) = \tau A(\alpha \cosh b + 2e^{-\Delta/T} a^{-1} \sinh b)/(1 - e^{-\Delta/T}), \tag{17}$$

and then combining Eqs. (16) and (17) gives

$$J(\pm d/2) = \alpha_\infty e^{-\Delta/T} \tau A(\alpha \cosh b + 2a^{-1} \sinh b)/(1 - e^{-\Delta/T}). \tag{18}$$

Equations (17) and (18) are sufficient to determine the total current J_t:

$$J_t(t) = J + \partial D/\partial t = J + i\omega\varepsilon_\infty E$$

$$= e^{i\omega t} \tau A e^{-\Delta/T}[\sigma_\infty(\alpha \cosh b + 2a^{-1} \sinh b)$$

$$+ i\omega\varepsilon_\infty(e^{\Delta/T}\alpha \cosh b + 2a^{-1} \sinh b]/(1 - e^{-\Delta/T}). \tag{19}$$

We still need to find the electric field E everywhere in the interval $-d/2 < x < d/2$ in order to determine $\langle E \rangle$. By integrating Eq. (7) and using Eq. (14) for $\rho(x)$, we find

$$E(x) = [(A/\alpha\varepsilon_\infty)\cosh(\alpha x) + E'], \tag{20}$$

where from Eq. (17) the constant of integration E' must be

$$E' = \tau A[\alpha \cosh b + 2e^{-\Delta/T} a^{-1} \sinh b]/(1 - e^{-\Delta/T}) - (A/\alpha\varepsilon_\infty)\cosh b. \quad (21)$$

Here, as in Eqs. (17) and (18), A (and thus ρ) must vanish as Δ goes to zero, but E can remain nonzero.

We point out that $J(x)$ can similarly be obtained within the interval:

$$J(x) = (-i\omega A\alpha^{-1}\cosh(\alpha x) + J'), \quad (22)$$

where from Eq. (18) the constant of integration J' must be

$$J' = \sigma_\infty e^{-\Delta/T}\tau A(\alpha \cosh b + 2a^{-1}\sinh b)/(1 - e^{-\Delta/T}) + i\omega A\alpha^{-1}\cosh b. \quad (23)$$

We see from Eqs. (21) and (23) that E and J are even functions of x, while ρ is odd. The x-dependences of these quantities are displayed in Figure 2.

We now find $\langle E \rangle$ and determine the conductivity $\sigma(\omega) = J_t/\langle E \rangle$. Integration of $E(x)$ from $-d/2$ to $d/2$ using Eq. (19) gives

$$\begin{aligned} \langle E \rangle &= E' + 2A\sinh b/\alpha^2\varepsilon_\infty \\ &= \tau A[(\alpha\cosh b + 2e^{-\Delta/T}a^{-1}\sinh b)/(1 - e^{-\Delta/T}) \\ &\quad - (b\cosh b - \sinh b)/(\alpha^2\tau\varepsilon_\infty d/2)]. \end{aligned} \quad (24)$$

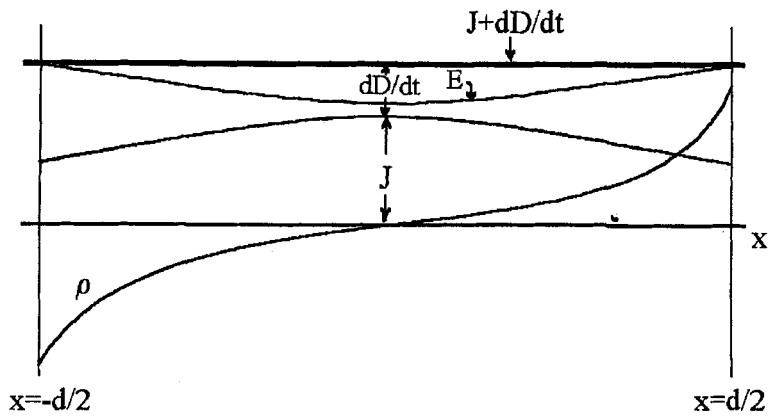

FIGURE 2 Typical spatial dependences of electric field E, current density J, displacement current density $\partial D/\partial t$, and net space charge density ρ between higher barriers.

Using the definition of α in Eq. (12), we find

$$1/\alpha^2\tau\varepsilon_{\infty} = \cos\phi\, e^{-i\phi}, \tag{25}$$

where $\phi = \tan^{-1}(\omega\varepsilon_{\infty}/\sigma_{\infty})$, so $\langle E\rangle$ in Eq. (24) can be written as

$$\langle E\rangle = \tau A[\alpha\cosh b + 2e^{-\Delta/T}a^{-1}\sinh b$$

$$- 2d^{-1}(1-e^{-\Delta/T})\cos\phi\, e^{-i\phi}(b\cosh b - \sinh b)]/(1-e^{-\Delta/T}). \tag{26}$$

Now we divide J_t by $\langle E\rangle$ to obtain the conductivity $\sigma(\omega)$:

$$\sigma(\omega) = \sigma_{\infty}[b\cosh b + r\sinh b + i\tan\phi(e^{\Delta/T}b\cosh b + r\sinh b)] \tag{27}$$

$$\bullet[e^{\Delta/T}b\cosh b + r\sinh b - (e^{\Delta/T}-1)\cos\phi\, e^{-i\phi}(b\cosh b - \sinh b)]^{-1}$$

SPECIAL CASES

This expression for the conductivity is rather complicated, so it is worth while to examine some special cases. First, if $\Delta = 0$,

$$\sigma(\omega)_{\Delta=0} = \sigma_{\infty} + i\omega\varepsilon_{\infty}, \tag{28}$$

as expected for a system with uncoupled conductivity and permittivity mechanisms.

Second, as angular frequency ω becomes large, we have $b \gg 1$ and $b \gg r$, so the $r\sinh b$ and $\sinh b$ terms in Eq. (27) are negligible. Also, $\sin\phi \simeq 1$ and $\cos\phi \simeq \sigma_{\infty}/\omega\varepsilon_{\infty} = 1/\tan\phi \ll 1$. Then, if $\exp(\Delta/T) \gg 1$, this high-frequency limit is

$$\sigma_{\text{hi-f}} \simeq \sigma_{\infty}(e^{-\Delta/T} + i\omega\varepsilon_{\infty}/\sigma_{\infty})/(1 + i\sigma_{\infty}/\omega\varepsilon_{\infty}) \simeq \sigma_{\infty} + i\omega\varepsilon_{\infty}. \tag{29}$$

This is the same result as in Eq. (28) for $\Delta = 0$, and shows that at frequencies high enough so that charges do not pile up against the high barriers, these barriers have negligible effect.

Third, in the dc limit of $\omega = 0$, we have $\sin\phi = \tan\phi = 0$ and $\cos\phi = 1$, so Eq. (27) reduces to

$$\sigma_{\text{dc}} = \sigma_{\infty}(b\cosh b + r\sinh b)/[b\cosh b + r\sinh b + (e^{\Delta/T}-1)\sinh b]. \tag{30}$$

In the usual situation that $b \gg 1$ so that $\sinh b \simeq \cosh b$, we obtain the following high- and low-temperature limits and crossover temperature T_x:

$$\sigma_{\mathrm{dc,hi-T}} \simeq \sigma_{\infty}, \tag{31}$$

$$\sigma_{\mathrm{dc,lo-T}} \simeq \sigma_{\infty}(b+r)\mathrm{e}^{-\Delta/T},$$

$$T_x \simeq \Delta/\ln(b+r).$$

This dc behavior can become complicated if there is a ferroelectric transition. For instance, if ε_{∞} obeys the Curie-Weiss law

$$\varepsilon_{\infty} = \varepsilon_0 C/(T - T_0) \tag{32}$$

above the Curie-Weiss temperature T_0, there could be three T_x values as temperature drops because $\alpha_{\mathrm{dc}} = (\varepsilon_{\infty}\tau)^{-1/2}$ and $b = \alpha d/2$. This would be manifested by the conductivity falling below the high-temperature Arrhenius law as temperature decreases, followed by a return to this law in the vicinity of T_0, as illustrated by curve A of Figure 3. In the simpler case of a Curie law ($T_0 = 0$ in Eq. (32)), the conductivity will merely exhibit a change in slope at T_x as shown by curve B of Figure 3.

Our fourth limiting case is for the dc permittivity ε'. It is determined from Eq. (27) by finding $\sigma''/\omega\varepsilon_0 = \varepsilon'$ in the limit of small but nonzero ω. In this limit, $\cos\phi \simeq 1$ and $\sin\phi \simeq \omega\varepsilon_{\infty}/\sigma_{\infty} = \tan\phi$ in Eq. (27). In the usual case that $b \gg 1$, $\sinh b \simeq \cosh b$ so these factors cancel in Eq. (27), which then reduces to

$$\sigma_{\omega\to 0} \simeq [\sigma_{\infty}(b+r) + i\omega\varepsilon_{\infty}(b\mathrm{e}^{\Delta/T} + r)]/$$
$$[\mathrm{e}^{\Delta/T} - 1 + b + r + i\{(\mathrm{e}^{\Delta/T} - 1)(b-1)\omega\varepsilon_{\infty}/\sigma_{\infty}\}]. \tag{33}$$

The imaginary part of Eq. (33) divided by $\omega\varepsilon_0$ yields

$$\varepsilon'_{\mathrm{dc}} = \varepsilon'_{\infty}[(b+r)^2 - 2r - b + 2r\mathrm{e}^{\Delta/T} + b\mathrm{e}^{2\Delta/T}]/(\mathrm{e}^{\Delta/T} - 1 + b + r)^2. \tag{34}$$

In the high-temperature limit the $(r+b)^2$ terms dominate, while in the low-temperature limit the largest exponential terms dominate. There is an intermediate temperature regime, rather than a crossover temperature as found

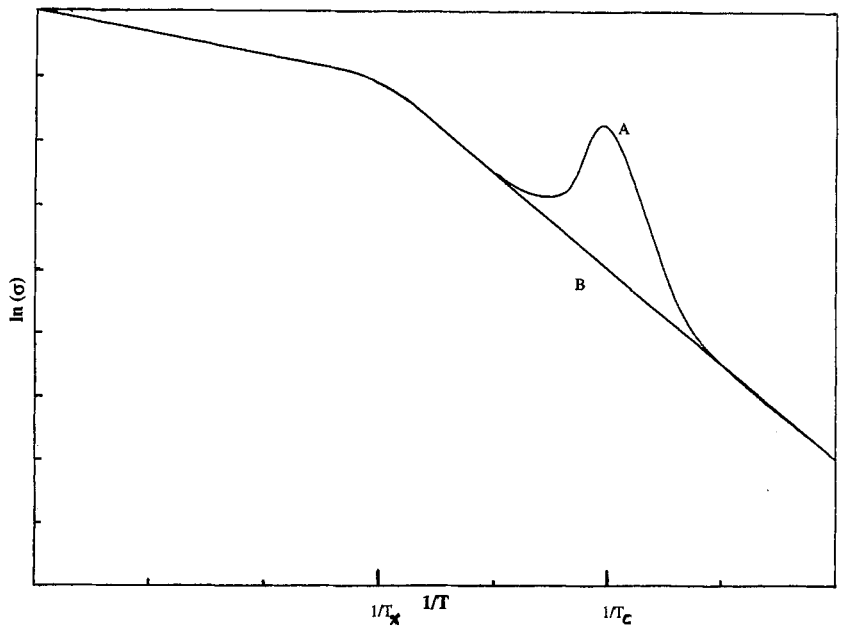

FIGURE 3 Typical temperature dependences predicted for dc conductivity. Curve A is for crystal obeying Curie-Weiss law. Curve B is for crystal without ferroelectric transition, obeying Curie law.

for the conductivity. These permittivity limits for different temperature ranges are:

$$\varepsilon'_{dc} \simeq \varepsilon'_{\infty} \qquad (\text{hi} - \text{T}) \qquad (b+r) \gg b^{1/2} e^{\Delta/T}, \tag{35}$$

$$\varepsilon'_{dc} \simeq \varepsilon'_{\infty} b e^{2\Delta/T}/(b+r)^2 \qquad (\text{crossover}) \qquad e^{\Delta/T} \ll (b+r) \ll b^{1/2} e^{\Delta/T},$$

$$\varepsilon'_{dc} \simeq \varepsilon'_{\infty} b = (\varepsilon'_{\infty}/\varepsilon_0 \tau)^{1/2} d/2 \qquad (\text{lo} - \text{T}) \qquad (b+r) \ll e^{\Delta/T}.$$

The high-temperature limit agrees with that found in Eq. (29), and may exhibit Curie-Weiss behavior as described in Eq. (32). The low-temperature limit then obeys a curious sort of square-root Curie-Weiss law. Very strong temperature dependence is predicted in the crossover region. Comparisons of these predictions with results[11] for strontium titanate are shown in Figure 4.

To find σ' and σ'' separately from Eq. (27) is quite complicated, because α and thus b are complex. In the usual case that $b \gg 1$, $\sinh b \simeq \cosh b$ so these factors cancel in Eq. (27). Then, upon multiplying numerator and denominator, of Eq. (27) by the complex conjugate of the denominator, we obtain the following expressions, in which the new denominator is designated DEN:

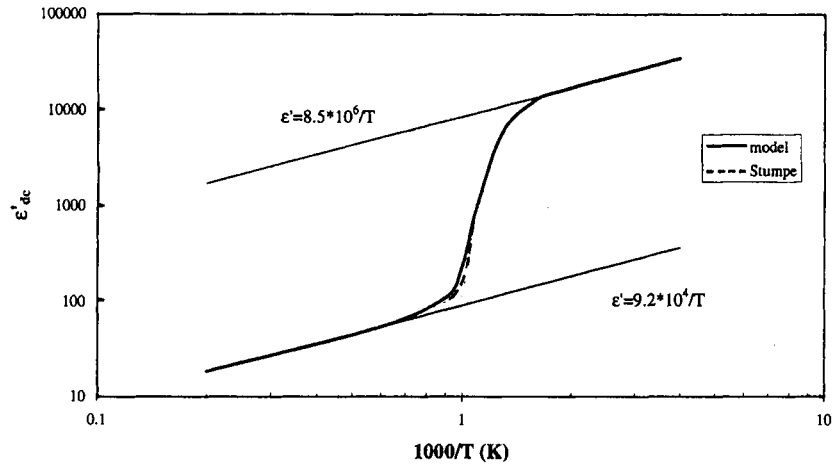

FIGURE 4 Typical temperature dependence predicted for dc permittivity. The low-frequency "dc" envelope of the data of Stumpe *et al.* (Ref. [1]) appears in the crossover region between the two Curie-law regimes.

$$\sigma' \simeq \{\sigma_\infty(b+r)[b\sin^2\phi e^{\Delta/T} + (e^{\Delta/T} - 1 + b)\cos^2\phi + r] \tag{36}$$

$$+ (be^{\Delta/T} + r)(\omega^2\varepsilon_\infty{}^2/\sigma_\infty)(e^{\Delta/T} - 1)\cos^2\phi(b-1)\}/\text{DEN};$$

$$\sigma'' \simeq \omega\varepsilon_\infty\{(e^{\Delta/T} + r/b)(b^2\cos^2\phi + br) - (e^{\Delta/T} - 1)(b^2\cos^2\phi + br\cos^2\phi)$$

$$+ (be^{\Delta/T} + r)b\sin^2\phi e^{\Delta/T} + (e^{\Delta/T} - 1)\cos^2\phi(be^{\Delta/T} + b + 2r)\}/\text{DEN};$$

$$\text{DEN} = [b\sin^2\phi e^{\Delta/T} + (e^{\Delta/T} - 1 + b)\cos^2\phi + r]^2$$

$$+ [(e^{\Delta/T} - 1)\cos^2\phi(b-1)\omega\varepsilon_\infty/\sigma_\infty]^2.$$

We see that σ' is positive, as required because negative σ' would correspond to a material *generating* electrical energy. To see that σ'' is positive, note that although the second term in the numerator is negative, each of its two factors is respectively smaller than the corresponding factor in the first term. Positive σ'' signifies that the sample is capacitive (positive ε') rather than inductive.

COMPARISON OF MODEL PREDICTIONS WITH EXPERIMENTAL RESULTS

The above discussion of special cases helps in understanding implications of the model, but we use the exact expression in Eq. (27) to make comparisons with the experimental results for $SrTiO_3$ single crystals obtained by Stumpe, Wagner, and Bäuerle[1]. We first try to fit their permittivity results for their thicker (1.02 mm) sample. These are more typical of results for a wide variety of materials, because there is not a second set of peaks as seen in their permittivity results for their thinner (0.24 mm) sample. Concurrently, we try to fit the conductivity results for their 0.24 mm sample, because they reported no conductivity results for their 1.02 mm crystal.

The best fits, in our opinion and not obtained by a best-fit procedure, are those shown in Figures 5 and 6. Note that although different sets of frequencies are used in these two figures, the same fitting parameters are used in both figures. They include: intrinsic barriers $B = 13000\,\mathrm{K}$ at spacing

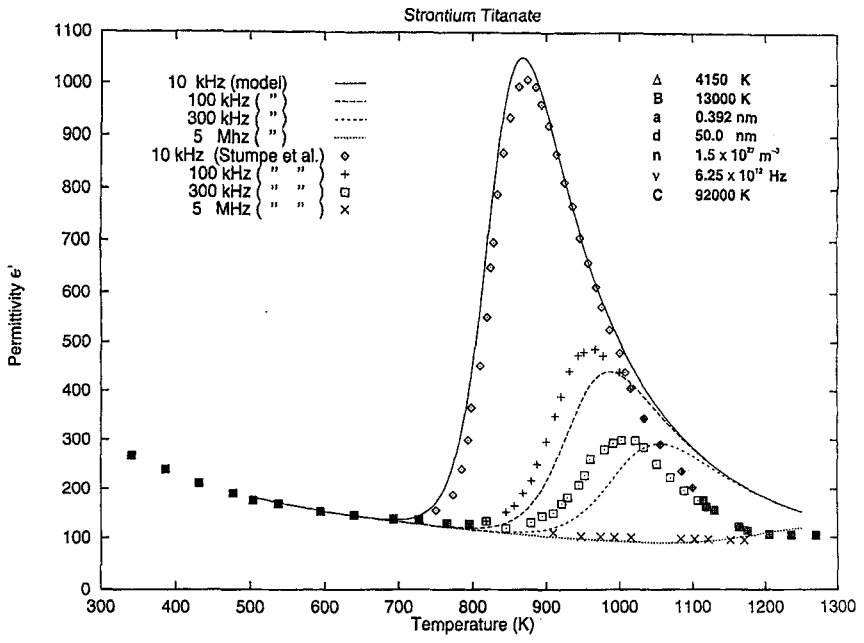

FIGURE 5 Fit to permittivity data of Stumpe *et al.* (Ref. [1]) for $SrTiO_3$ crystal 1.02 mm thick.

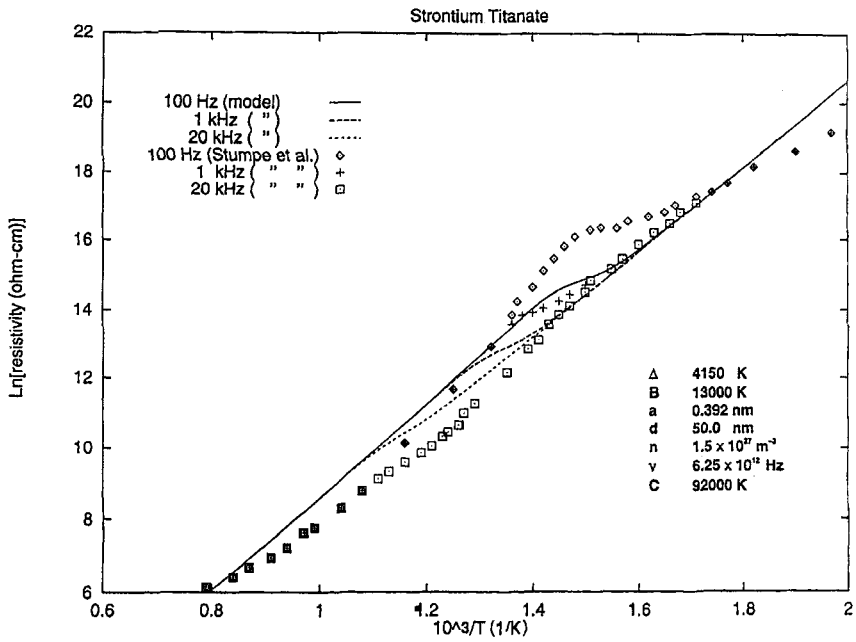

FIGURE 6 Fit to permittivity data of Stumpe *et al.* (Ref. [1]) for $SrTiO_3$ crystal.

$a = 0.4$ nm, extrinsic barriers $\Delta = 4150$ K at spacing $d = 50$ nm, carrier concentration $n = 1.5 \times 10^{27}/\text{m}^3$, and Debye temperature $\Theta = 300$ K.

The permittivity fit, although not exact, is surprisingly close to experiment. It shows all the observed features: A high-frequency Curie-law envelope, a low-frequency envelope which is in the crossover regime of Figure 4, and dielectric peaks at temperatures which increase with increasing frequency.

The conductivity fit also shows the observed features of high- and low-frequency envelopes which extrapolate to meet at finite temperature, and crossover between these envelopes for which the temperature dependence of conductivity at a given frequency is quite weak.

A direct comparison of the predicted permittivity and conductivity results is provided by the Cole-Cole plots in Figure 7 for three temperatures. At high frequencies these curves begin like Debye relaxation plots, but as frequency decreases, the center of the semicircle shifts below the real axis. Finally at the lowest frequencies, the curve shoots up steeply because of domination by the dc conductivity mechanism. As temperature decreases, a greater part of the distorted semicircle appears.

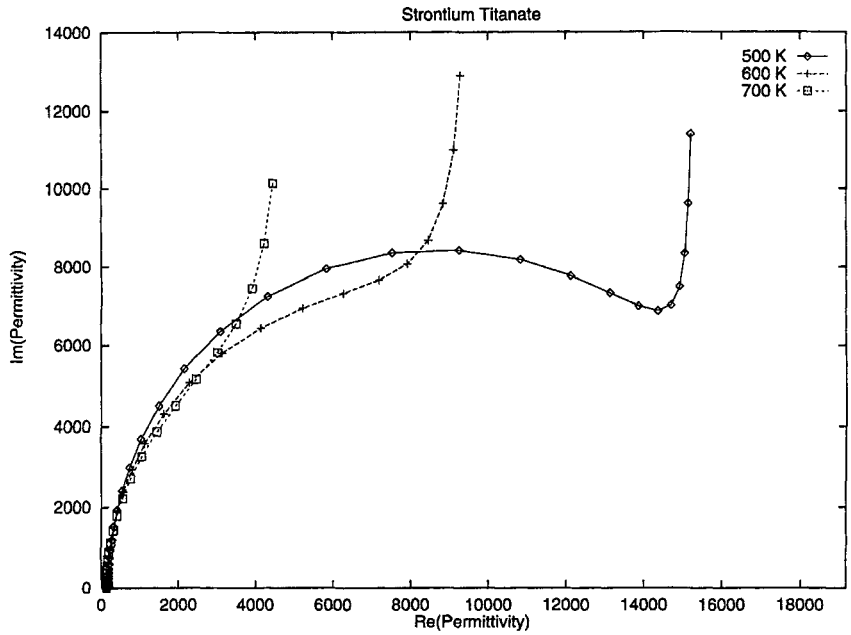

FIGURE 7 Cole-Cole plots for model parameters used for fits in Figures 5 and 6.

Now that we have seen that the model with two barrier heights (B and $B+\Delta$) gives quite good fit for the permittivity of the 1.02 mm sample, we can ask whether adding a second set of extrinsic barriers of height $B+\Delta+\Delta_2$ and of spacing $d_2 \gg d$ can fit the 0.24 mm sample permittivity results. In this case, we would let $d_2 = 0.24$ mm so that the highest barriers represent surface barriers which might account for the second set of permittivity peaks seen by Stumpe *et al.*[1] and reproduced in Figure 8.

To accommodate this third set of barriers, we generalize the two-barrier-height model so that each continuum region has length d_2 instead of d. In Eq. (3) we replace σ_∞ by $\sigma'(\omega)$ found in the previous iteration in which the highest barriers had height $B+\Delta$. Similarly, in Eq. (7) we replace ε_∞ by $\varepsilon_0\varepsilon'(\omega) \equiv \sigma''(\omega)/\omega$ found in the $B+\Delta$ iteration. The justification for this procedure is that the conductivity and permittivity in the larger d_2 intervals are modified by the $B+\Delta$ barriers within these intervals. Added justification comes from generalizing the result found for $B+\Delta$ highest barriers, that if σ_∞ and ε_∞ are real and positive, so are $\sigma'(\omega)$ and $\varepsilon'(\omega)$. The generalization then insures that $\sigma'_2(\omega), \sigma'_3(\omega), \ldots$, and $\varepsilon'_2(\omega), \varepsilon'_3(\omega), \ldots$ will also be real and positive.

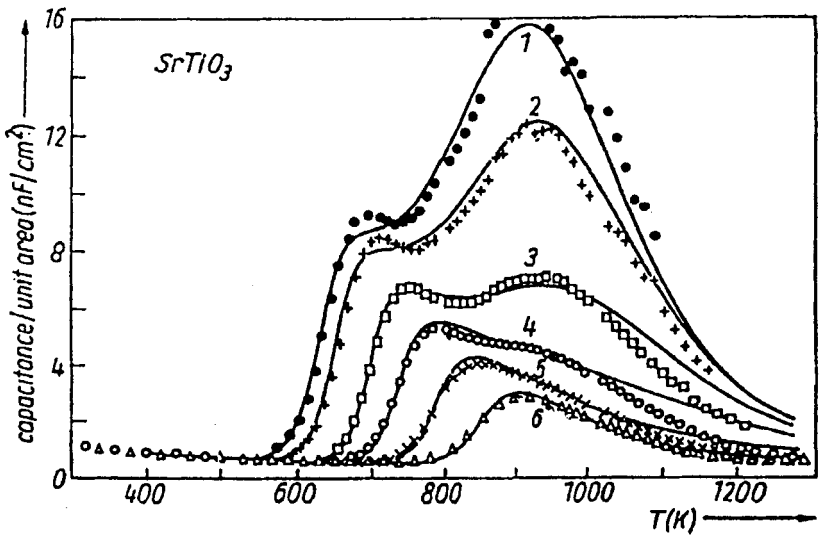

FIGURE 8 Permittivity data of Stumpe *et al.* (Ref. [1]) for crystal 0.24 mm thick.

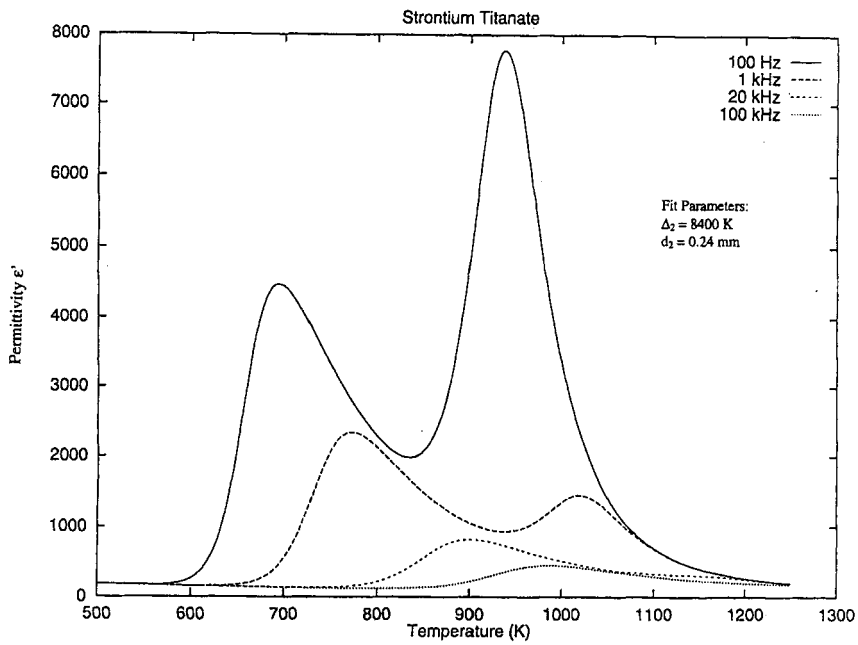

FIGURE 9 Calculated permittivity for comparison with data of Figure 8, using model with third set of barriers with spacing equal to crystal thickness of 0.24 mm.

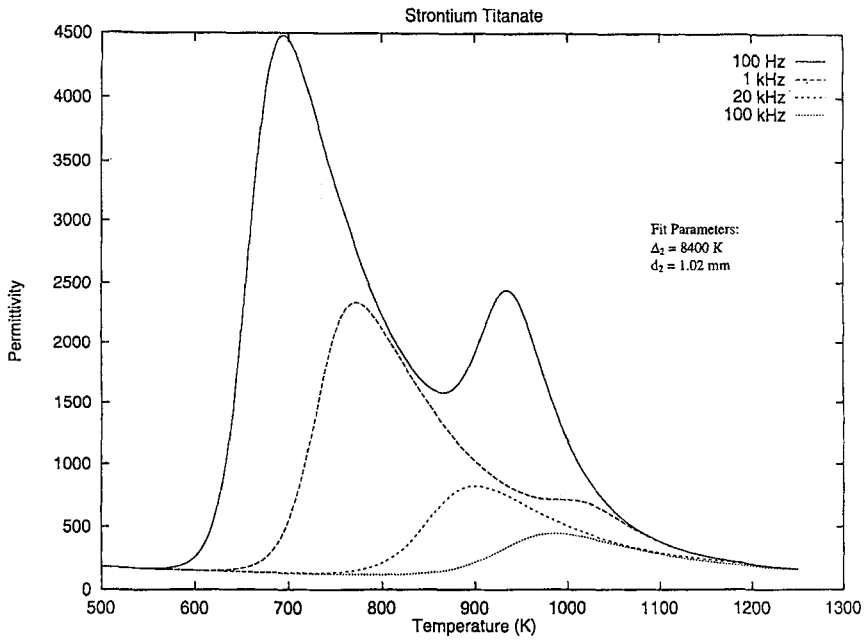

FIGURE 10 Calculated permittivity with all parameters same as in Figure 9, except third barrier set spacing is 1.02 mm.

The results from incorporating this second set of extrinsic barriers are shown in Figures 9 and 10. The barrier heights B and $B+\Delta$, and the spacing d, are the same as before. We see that the lower-temperature set of permittivity peaks is essentially unaffected, but another set of peaks of comparable peak width and frequency dispersion appears.

In comparing with the experimental data[1] for a $SrTiO_3$ crystal 0.24 mm thick, similarities and differences can been seen. The similarities are that a second peak appears, and gets weaker both as frequency increases and as the crystal becomes thicker. The second peak is not evident in the data in Figure 5 for a crystal 1.02 mm thick, because Stumpe *et al.* chose a higher frequency range for this crystal than for the 0.24 mm crystal.

The differences are that Stumpe *et al.*'s higher-temperature peaks are broader and show less frequency dispersion than our model pridictions. Both these effects could result from a distribution of activation energy $B+\Delta+\Delta_2$ over the area of the contact electrodes.

The addition of the second set of extrinsic barriers of height $B+\Delta+\Delta_2$ has a less dramatic effect on the conductivity $\sigma'(\omega,T)$ and is not pictured here.

CONCLUSIONS

In summary, our two-barrier-height model with intrinsic barriers of height B and spacing a, and extrinsic barriers of height $B+\Delta$ and spacing d, fits temperature- and frequency-dependent conductivity and permittivity data of Stumpe, Wagner and Bäuerle[1] for a strontium titanate single crystal of width 1.02 mm quite well. Addition of a second set of barriers with spacing equal to the crystal width gives some features of the second set of peaks seen for their thinner (0.24 mm) crystal.

From these results, it appears probable that these crystals exhibit phase-shifted conductivity due to extrinsic carriers, whose mobility is limited by intrinsic barriers at short intervals of the order of a lattice spacing, by higher extrinsic barriers of spacing of order 50 nm, and by still higher surface barriers.

As discussed in the Introduction, these effects of phase-shifted conductivity appear in many other perovskite crystals and ceramics. Our next task is to try to fit these other results, using Curie-Weiss or other appropriate behavior for ε_∞, instead of the simpler Curie-law behavior appropriate to strontium titanate. Another task is to look for behavior predicted by the model but not yet observed, namely the low-temperature decrease in the slope of the dc permittivity *vs.* temperature curve.

This work was supported by NSF Grant DMR-9520251.

References

[1] Stumpe, R., Wagner, D. and Bäuerle, D. (1983). *Phys. Stat. Sol. (a)*, **75**, 143.
[2] Bidault, O., Goux, P., Kchikech, M., Belkaoumi, M. and Maglione, M. (1994). *Phys. Rev. B*, **49**, 7868.
[3] Kuwabara, M., Goda, K. and Oshima, K. (1990). *Phys. Rev. B*, **42**, 10012.
[4] Tu, C.-S., Siny, I. G. and Schmidt, V. H. (1994). *Phys. Rev. B*, **49**, 11550.
[5] Schmidt, V. H., Tu, C.-S. and Siny, I. G. (1995). IEEE Publ. CH3416-5 0-7803-1847-1/95, Proc. of Internat. Symposium on Applications of Ferroelectrics (*ISAF94*), p. 45.
[6] Schmidt, V. H., Tuthill, G. F., Tu, C.-S., Schogoleva, T. V. and Meschia, S. C. (1996). *J. Phys. Chem. Solids*, **57**, 1493.